Modeling gas flow in a looped thermosyphon with a 1 D low-Mach number expansion

Giuseppe Parasiliti Rantone[1], Nora Aïssiouene[2], Yohan Penel[3,4], and Pierre-Yves Lagrée[1]

[1]Sorbonne Université, CNRS UMR 7190, Institut Jean Le Rond d'Alembert, F-75005 Paris, France
[2]Sorbonne Université, Sorbonne Université Maison des Modélisations, Ingénieries et technologies, SUMMIT, F-75005 Paris, France
[3]Sorbonne Université, CNRS, Université de Paris Cité, INRIA, Lab. Jacques-Louis Lions (LJLL), F-75005 Paris, France
[4]Inria, team ANGE, 2 rue Simone Iff, 75012 Paris, France

July 16, 2025

Abstract

This article provides numerical results for a laminar gas flow at small velocities in the "looped thermosyphon", or "natural circulation loop" : a closed configuration composed of two horizontal adiabatic pipes and two vertical pipes with different fixed wall temperature. To this extent, following Paolucci, [39, 40] we construct a low-Mach number model capable of taking into account the periodicity and the discontinuities intrinsic to this configuration. This compressible model is richer than the Boussinesq model since it describes the pressure variation and is adapted to the description of flows driven by large temperature gradients. We settle averaged equations through the pipes of small radius compared to the length, this gives a one dimensional system of equations of mass, momentum and energy with two pressures, a dynamical one and a thermodynamical one only function of time. We construct a quasi-exact solution in a laminar and steady-state regime. We approach the low-Mach averaged 1D Model with a coupled numerical method based on the characteristics method considering the presence of the periodic conditions and the discontinuous gravity term with Dirac distributions as derivatives at the corners. The numerical results are confronted

and validated by the aforementioned reference solution to determine their accuracy.

keywords: gas flow, low-Mach assumption, thermosyphon simulation, single-phase natural circulation loop, reference solution, periodic conditions, computational fluid dynamics.

Table 1: Nomenclature

Description	**Symbol**	**Unit**
Courant–Friedrichs–Lewy number	CFL	–
Specific heat at constant pressure	C_p	$\mathrm{m^2{\cdot}s^{-2}{\cdot}K^{-1}}$
Pipe diameter, Radius	D, R	m
Rate of strain tensor	D	$\mathrm{s^{-1}}$
Modified Fannig	f	$\mathrm{m{\cdot}s^{-1}}$
Heat transfer coefficient	h	$\mathrm{kg{\cdot}s^{-3}{\cdot}K^{-1}}$
Thermal conductivity	k	$\mathrm{kg{\cdot}m{\cdot}s^{-3}{\cdot}K^{-1}}$
Loop length	L	m
Mean pressure across section	p	$\mathrm{kg{\cdot}m^{-1}{\cdot}s^{-2}}$
Thermodynamic pressure function of time	$P(t)$	$\mathrm{kg{\cdot}m^{-1}{\cdot}s^{-2}}$
Radial coordinates	r	m
Specific gas constant	r	$\mathrm{m^2{\cdot}s^{-2}{\cdot}K^{-1}}$
Pipe Surface	S	$\mathrm{m^2}$
Time	t	s
Mean temperature across section	$T(x,t)$	K
Cold temperature	T_c	K
Fluid temperature	T_f	K
Longitudinal velocity	$u_x(x,r,t)$	$\mathrm{m{\cdot}s^{-1}}$
Mean longitudinal velocity	$u(x,t)$	$\mathrm{m{\cdot}s^{-1}}$
Longitudinal coordinate	x	m
Heat capacity ratio	γ	–
Angle of the pipe	θ	-
Dynamic viscosity	μ	$\mathrm{kg{\cdot}m^{-1}{\cdot}s^{-1}}$
Dynamic pressure	Π	$\mathrm{kg{\cdot}m^{-1}{\cdot}s^{-2}}$
Density	$\rho(x,t)$	$\mathrm{kg{\cdot}m^{-3}}$
Shear stress at the wall	τ_x	$\mathrm{s^{-1}}$

1 Introduction

Modeling gas flows in a network of heated or cooled pipes is crucial in a wide range of engineering applications. We are interested in cases where the gas velocity is low enough that the Mach number remains much smaller than one—a condition frequently encountered in practical systems. Such low-speed gas flows occur in many industries involving gas transport through pipelines and complex pipe networks. In particular, the increasing demand for the transportation of liquefied natural gas (LNG) has raised numerous questions about the behavior of gas flows in pipe systems subjected to temperature variations. One of the most simple archetypal flow problems in an arrangement of pipes with heat exchange is the "thermosyphon" or "natural circulation loop" (see Figure 1 for a schematic representation). The looped thermosyphon is a closed pipeline configuration of length $4L$ where the gas is confined at some mean pressure in the gravity field and flows in a loop (here, a square) from one tube to another. The one at temperature T_f cools the gas, making it denser causing it to descend, while the one at temperature T_c heats it, making it less dense and consequently move up. The two remaining segments are adiabatic, with no heat exchange. These combined thermal effects drive a continuous, buoyancy-induced circulation. We will study this configuration in curvilinear coordinates with the axial coordinate x, taking values in $[0, 4L]$. The point $x = 0$ is the bottom left corner, corresponding with the inlet of the heated pipe. As the domain is closed with periodic boundary conditions, the points $x = 0$ and $x = 4L$ coincide. Moreover, the outlet of every pipe coincides with the inlet of the contiguous pipe.

The most common approximation of the Navier-Stokes equations assuming little overall density variations is the Boussinesq model [8]; this is equivalent to the hypothesis of incompressible flow (null velocity divergence) and small variations of pressure and temperature. Pressure remains close to the hydrostatic pressure and there is a linear relation between density and temperature variations. Furthermore, "density variations are neglected where they are not multiplied by gravity g" as stated historically by Boussinesq in [8]. One can indeed find in the literature both experimental studies and numerical simulations based on a Boussinesq assumptions for configurations similar to the thermosiphon described above. These works are often motivated by industrial applications, aiming at specific analyses of temperature behavior. Some examples are given in [27, 24, 13, 6, 46, 11].

Concerning the simulation of gas flows, several works tackle configurations far more complex than the thermosyphon. Analyzing the most common choices in physical, mathematical, and numerical modeling is still useful. A common issue is dealing with non-linear conservative hyperbolic equations; it is common to simplify some terms in the momentum equations such as the non-linear or the gravity terms; usual choices are a Boussinesq or an isothermal assumption, see for

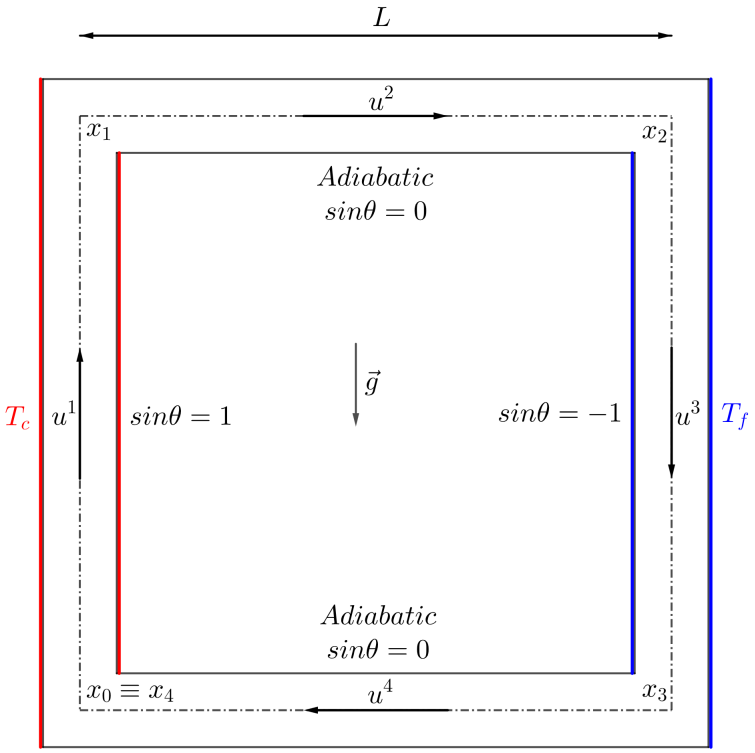

Figure 1: A sketch of the geometry of the looped thermosyphon (natural circulation loop): a closed pipe of length $4L$ where the gas is confined and flows between the temperatures T_f (cooled, it is denser, and falls) and T_c (heated, it is less dense and moves up). The inclination of the pipes θ depends on the geometry: in the heated pipe is $\frac{\pi}{2}$, in the cooled one is $-\frac{\pi}{2}$ and in the others 0 and π.

example [16, 22, 26, 37]. A frequent choice is to use an averaged one-dimensional model instead of the full three-dimensional one and to simplify the momentum equation as in [36, 26, 44]. They neglect the non-linear and the inclination terms and do not use the energy equation; the former carries on the simulation through an electrical analogy, while the latter uses a transfer function model coupled with a linear interpolation of available temperature measurements instead of the energy equation. Another application of an electrical analogy is proposed by [12], [21] and [34] explore some alternatives. Concerning the numerical schemes, it is possible to use finite differences combined with the method of characteristics as in [36]. In contrast, others have made some comparisons between finite differences and finite elements, like [18] and [52] or used only finite elements like [20].

In 1982, to add compressibilily effects to the Boussinesq model, Paolucci introduced an alternative approach to remove the compressible effect of sound waves (much faster than the average fluid flow) from the governing equations [39]. He

obtained a "low-Mach number" model for the three-dimensional Navier-Stokes equations for general domains by means of an asymptotic analysis of the low-Mach limit. One of the key features of Paolucci's approach is the splitting of the pressure into two terms: a thermodynamic one taking into account global compressible effects (only function of time, not on space, noted $P(t)$) of the dominant order and function of temperature only and a dynamic one associated to velocity changes (noted Π, function of space and time) of the order of magnitude of squared Mach, function of temperature and position. This model is then applied to studying a differentially heated cavity [40], the first of many works on the differentially heated cavity with a low-Mach model. In [28], they derive numerical reference solutions for steady natural convection flows by varying the Rayleigh number and the viscosity law. In [38], we see the effort of performing low-Mach simulations through different methods, using an asymptotic expansion and developing an algorithm for the fully compressible Navier-Stokes equations with particular attention to the discretization when the Mach number is low. Over time the assumption of low-Mach number has been extended to more complex physical problems like in [1, 47, 7, 25]. During the last decades, the low-Mach model has greatly interested the scientific community. For example [42, 4, 32, 30, 41, 35, 31, 23, 51] apply this approximation in many fields. Recently in [45], we can see how to extend to low-Mach regimes the methods for reduced models through proper orthogonal decomposition of Navier-Stokes equations coupled with thermal effects. In [10] they perform an asymptotic analysis combining the asymptotic limit of several small parameters, including the Mach number.

We have seen how, in pipe flows, the state of the art is Boussinesq-based and how the low-Mach assumption is employed in many fields. In this paper, we develop Paolucci [40] approach by applying the low-Mach expansion in a complex geometric configuration with corners and periodicity.

The paper is organized as follows: in section 2, we derive an unsteady and one-dimensional low-Mach model inspired from Paolucci for pipe flows based on an asymptotic expansion. In particular, we exploit the small gas velocity to have the Mach number tending to zero and apply the tools of perturbation theory to obtain a simplified model. Additionally, we summarize the features of the Boussinesq model and show the differences with the low-Mach model. In section 3, we construct a laminar steady reference solution for pipes. In section 3.2 we see how to construct an analytical solution for the thermosyphon at constant kinematic viscosity. Additionally, we prove on the thermosyphon the classical limit of our model for small temperature differences. In section 4, we present the numerical algorithm we have implemented and explain how the discontinuities of the gravity term give issues to the simulation and how we addressed them. In section 5, we show some numerical results (compared with the analytical solution)

obtained with the implementation of our algorithm.

2 The model

2.1 Thin layer compressible Navier-Stokes

We consider the compressible, laminar flow of a Newtonian ideal gas in a pipe of radius R and length L. The pipe has an angle of inclination θ with horizontal, the gravitational acceleration is g (see figure 2).

Thermodynamical coefficients are supposed constant. The specific heat capacity at constant pressure is C_p, the thermal expansion coefficient $\alpha = (-\frac{1}{\rho}\left.\frac{\partial \rho}{\partial T}\right|_p) = 1/T$ for ideal fluid. The ratio γ of the heat capacity at constant pressure C_p to the heat capacity at constant volume C_v, allows to write $C_p := \frac{\gamma \mathrm{r}}{\gamma - 1}$ with r specific contant of the gas.

The flow is assumed to be axisymmetric, r is the radial coordinate.The compressible Navier–Stokes equations are non-dimensionalized using the classical Reynolds number Re, Mach number Ma, Froude number Fr, and Prandtl number Pr. Assuming the pipe is slender, with $R/L \ll 1$, the equations can be simplified to a thin-layer Navier–Stokes system. In this limit, longitudinal second-order derivatives in the momentum and energy equations can be neglected, and the pressure is therefore uniform in the radial direction. This leads to a system analogous to the axisymmetric boundary layer equations, as described in [48].

The resulting system remains two-dimensional. We integrate those equations across the section as usual to obtain one-dimensional equations. This averaging technique is classical and is used in many thin layer configurations in fluid mechanics (compressible flow in pipes [21], shallow water equations, [50], flow in arteries [19]...). The thin layer compressible Navier-Stokes section-averaged system written back with dimensions and using $I_S(u_x) := \int_0^R 2\pi u_x(x,r,t) r \mathrm{d}r$ as a shorthand reads:

$$\frac{\partial}{\partial t} I_S(\rho) + \frac{\partial}{\partial x} I_S(\rho u_x) = 0, \tag{1a}$$

$$\frac{\partial}{\partial t} I_S(\rho u_x) + \frac{\partial}{\partial x} I_S(\rho u_x^2) + \frac{\partial}{\partial x} I_S(p) = -\tau_w \pi D - \rho S g \sin\theta, \tag{1b}$$

$$\rho C_p \left(\frac{\partial}{\partial t} I_S(T) + \frac{\partial}{\partial x} I_S(T u_x) \right) = \alpha \left(\frac{\partial}{\partial t} I_S(p) + \frac{\partial}{\partial x} I_S(p u_x) \right) + I_S(\tau : \mathrm{D}) - 2\pi R q_w, \tag{1c}$$

$$\rho = \frac{p}{\mathrm{r}T}, \tag{1d}$$

The 1D system (1) is function of space variables x and time variable t. It is constituted of (1a) the averaged continuity equation, (1b) the averaged momen-

tum equation, (1c) the averaged temperature (or energy) equation, and (1d) the equation of state (ideal gas law).

The final unknowns are defined as an integral on the cross-section of the pipe. For example, the mean value of velocity is defined as :

$$u(x,t) = \frac{I_S(u_x(x,r,t))}{\int \mathrm{d}S} = \frac{\int u_x(x,r,t)\mathrm{d}S}{S}.$$

For pressure $p(x,t)$, due to the thin layer approximation, its mean value coincides with itself $I_S(p(x,t)) = p(x,t)$. For quantities that vary on the cross-section, such as velocity, density and temperature, one has to provide additional hypotheses on the profile. These assumptions allow us, for example, to link $\int u_x^2 r\mathrm{d}r$ to Su^2 (through the Coriolis-Boussinesq coefficient). This procedure is discussed in Shallow Water flows [50], in arterial flows [19], and in thermal flows [3]. It is possible to suppose a plug flow (constant velocity with r) or a Poiseuille flow [33, 14] in which the velocity is supposed parabolic along the radial axis. The first one is more suitable for high Reynolds flows, and the second one is more suitable for lower Reynolds flows, neglecting all entrance effects in both cases. In the case of a Poiseuille profile, $I_S(u_x^2) = (4/3)u^2S$. In practice (even if it is valid only for plug flows), we will say that $I_S(u_x^2) = u^2S$, as it is common for pipe flows [19]. The area of the pipe cross-section is $S = \int_0^R 2\pi r\mathrm{d}r = \pi R^2$, but few extra hypotheses allow extend to any cross sections; hence D is the hydraulic diameter (and R the hydraulic radius).

In the same vein, to estimate shear stress at the wall τ_w and dissipation $I_S(\tau : \mathrm{D}) = \int \tau_{ij}D_{ij}\mathrm{d}S$ as function of mean value of velocity $u(x,t)$, one has to do the same hypothesis on velocity profile. The general expression for τ_w at the wall is linked to $u(x,t)$ by the tabulated Fanning friction coefficient : $\tau_w/\frac{\rho u^2}{2}$. In the case of laminar flow, $\tau_w = \frac{4\mu u}{R} = \frac{\frac{8\nu}{R}}{2}\rho u$. We suppose in the following kinematic viscosity $\nu := \frac{\mu}{\rho}$ to be constant (as a first approximation) and subsequently defined a modified Fanning coefficient as $f := \frac{8\nu}{R}$. The constant ν assumption will help construct the analytical solution. Relaxing this hypothesis for the numerical computations will not be a problem. The source term of the Heat Equation $I_S(\tau_{ij}D_{ij}) = \int \pi 2\mu r \left(\frac{\partial u_x}{\partial r}\right)^2 \mathrm{d}r$ may be computed in the case of the Poiseuille flow and gives $\pi\tau_w D$.

Finally, using the definition of the Nusselt number and the results of the Graetz problem [29, 43], we introduce the classical [53] heat exchange coefficient h to model exchanges with the wall. We note that the temperature is the velocity-averaged temperature in the Graetz problem. By considering a reference temperature T_{ref}, the heat flow through the lateral surface of the pipe is :

$$q_w(x,t) = h(T(x,t) - T_{ref}).$$

Hence the values at the wall τ_w and q_w and the bulk value $I_S(\tau_{ij}D_{ij})$ are linked to the associated mean fields $u(x,t)$ and $T(x,t)$ through empirical relations.

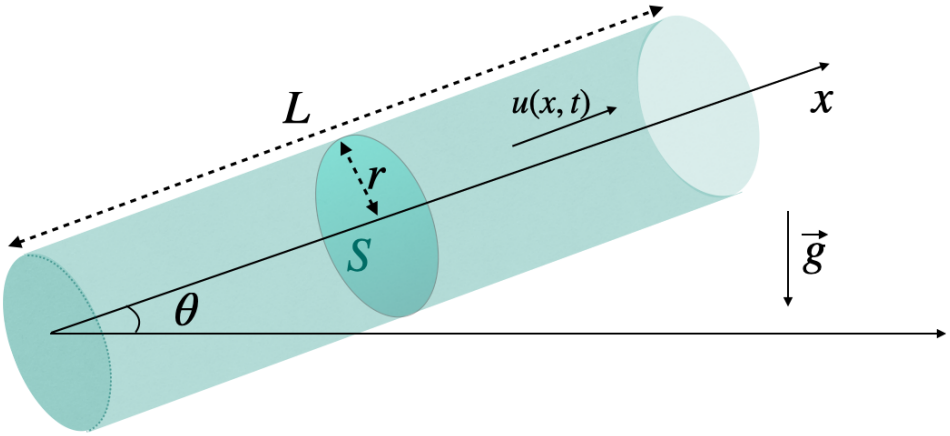

Figure 2: Sketch of an oriented inclined pipe of length L, cross-section S, and inclination angle θ, with mean axial velocity $u(x,t)$ in a gravity field $\vec{g}$.

2.2 The low-Mach model

In many practical industrial applications, the gas velocity is small compared to the speed of sound c, which implies that the Mach number (Ma) is small. This can present a singularity when working with the dimensionless momentum equation (1b), due to the presence of the Ma^{-2} scaling in front of the pressure term: $(\frac{1}{\gamma Ma^2}\frac{\partial(\tilde{S}\tilde{p})}{\partial\tilde{x}})$. The dimensionless version of momentum equation (1b) is indeed :

$$\frac{\partial(\tilde{S}\tilde{\rho}\tilde{u})}{\partial\tilde{t}} + \frac{\partial(\tilde{S}\tilde{\rho}\tilde{u}^2)}{\partial\tilde{x}} + \frac{1}{\gamma Ma^2}\frac{\partial(\tilde{S}\tilde{p})}{\partial\tilde{x}} = -\frac{f}{2}\pi\tilde{\rho}\tilde{u}\tilde{D} - \frac{1}{Fr}\tilde{S}\tilde{\rho}\sin\theta. \tag{2}$$

Following Paolucci [39, 40], a low-Mach-number model can be derived by performing an asymptotic expansion of the flow variables under the assumption $Ma \to 0$. The expansions are as follows:

$$\tilde{u}(x,t) = \tilde{u}_0(x,t) + Ma\tilde{u}_1(x,t) + \mathcal{O}(Ma^2), \tag{3a}$$
$$\tilde{T}(x,t) = \tilde{T}_0(x,t) + Ma\tilde{T}_1(x,t) + \mathcal{O}(Ma^2), \tag{3b}$$
$$\tilde{p}(x,t) = \tilde{P}_0(x,t) + Ma\tilde{P}_1(x,t) + \gamma Ma^2\tilde{\Pi}(x,t) + \mathcal{O}(Ma^3). \tag{3c}$$

Substituted in the equations without dimension gives at the order Ma^{-2} and Ma^{-1} for the momentum equation (2):

$$\partial_{\tilde{x}}\tilde{P}_0 = 0, \quad \partial_{\tilde{x}}\tilde{P}_1 = 0.$$

At order $\mathcal{O}(Ma^{-2})$, the pressure is spatially uniform and hence is only function of time. When dimensional variables are reintroduced, this corresponds to the thermodynamic pressure $P(t)$. At order $\mathcal{O}(Ma^{-1})$, the perturbation in space and time will remain null by boundary conditions. At the next order, $\mathcal{O}(1)$, the pressure gradient reappears in the momentum equation as: $\frac{1}{\gamma Ma^2}\frac{\partial(\tilde{S}\tilde{p})}{\partial\tilde{x}} = \frac{\partial(\tilde{S}\tilde{\Pi})}{\partial\tilde{x}}$. Re-introducing the dimensional variables, equation (1a) is not changed, equation (1b) is with the dynamic pressure Π, and equation (1c) has the thermodynamic $P(t)$ in it. The resulting form of the 1D low-Mach number model is:

$$\frac{\partial(Su)}{\partial x} = -\frac{S}{\rho}\left(\frac{\partial\rho}{\partial t} + u\frac{\partial\rho}{\partial x}\right), \tag{4a}$$

$$\frac{\partial(S\rho u)}{\partial t} + \frac{\partial(Su^2\rho)}{\partial x} + \frac{\partial(S\Pi)}{\partial x} = -\frac{f}{2}\pi\rho u D - \rho S g\sin\theta, \tag{4b}$$

$$\rho C_p\left(\frac{\partial(ST)}{\partial t} + u\frac{\partial(ST)}{\partial x}\right) = SP'(t) - 2\pi R q_w, \tag{4c}$$

where $P(t)$ is the thermodynamic pressure involved in the energy equation, while $\Pi(x,t)$ (the second order perturbation) is the dynamic pressure involved in the momentum equation.

Always following Paolucci, different formulation of the divergence equation (4a) can be settled, using the identity $d\rho = \frac{\partial\rho}{\partial T}dT + \frac{\partial\rho}{\partial P}dP$, and taking into account of (4c), the (4a) equation reads:

$$\frac{\partial(Su)}{\partial x} = A(T,P)P'(t) + B(T,P)q_w. \tag{5}$$

In the case of ideal gases, A and B reduce to:

$$A(T,P) := -\frac{S}{\gamma P}, \quad B(T,P) := -\frac{2\pi R(\gamma-1)}{\gamma P}. \tag{6}$$

By the periodicity of the closed domain (the four closed pipes) of length $4L$

$$\int_{\text{domain}} \partial_x(Su)\,\mathrm{d}x = 0, \text{ therefore } \int_{\text{domain}} (A(T,P)P'(t) + B(T,P)q_w)\,\mathrm{d}x = 0.$$

It gives the following equation for the time evolution of thermodynamic pressure :

$$P'(t) = -\frac{\int_{\text{domain}} B(T,P)q_w\,\mathrm{d}x}{\int_{\text{domain}} A(T,P)\,\mathrm{d}x} = -\frac{2\pi R(\gamma-1)}{4SL}\int_{\text{domain}} q_w\,\mathrm{d}x, \tag{7}$$

This relation represents the variations of thermodynamic pressure due to the heating (in Boussinesq approximation, it is zero).

Remark.

For numerical resolution of pressure Π, an additional equation (9) deduced from (4b) is useful for the numerical implementation. Taking the derivative of from (4b) with respect to x, it gives a kind of Poisson equation with source terms. In the source terms are terms in derivative of u, we define the longitudinal shear as a new variable (which is not null as in Boussinesq, Paoluci [39]):

$$s_x := \frac{\partial u}{\partial x} = -\frac{1}{\gamma P(t)}\left(P'(t) + \frac{2\pi R(\gamma-1)}{S} q_w\right), \tag{8}$$

those terms will appear between brackets in the final expression (9). In the source terms are as well terms coming from the derivative of $\sin\theta$ at each change of direction, in the case of the thermosyphon, the values of $\sin\theta$ are 1,0-1,0, (Figure 1), so that a sum of four δ Dirac Deltas distributions will appear with weights (say in general ξ_i corresponding to the magnitude of the discontinuous changes from one pipe to the other at each of the four corners). The equation is :

$$-\partial_x\left(\frac{\partial_x \Pi}{\rho}\right) = \left[\partial_t s_x + u\partial_x s_x + s_x^2 + \frac{f\pi s_x D}{2S}\right] + g\sum_{i=1}^{4}\xi_i\delta_{iL}. \tag{9}$$

This continuous formulation highlights the type of equation to be solved. In the following, we adopt a semi-discretization in time, upon which a splitting method inspired by the Chorin–Temam projection approach is applied. The numerical scheme is described in section (4).

2.3 The Boussinesq model

In this section, we revisit the Boussinesq model to highlight its key differences from the low-Mach-number model. In particular, the counterpart of equation (4a) has no source term leading to the simplified form $\partial_x(Su) = 0$, and in heat equation there is no $P'(t)$ contribution, only convection and diffusion. Then the counterpart of (4a), (4b) and (4c) is the laminar 1D averaged Boussinesq problem:

$$\frac{\partial(Su)}{\partial x} = 0, \tag{10a}$$

$$\rho_c\left(\frac{\partial(Su)}{\partial t} + \frac{\partial(Su^2)}{\partial x}\right) + \frac{\partial(Sp)}{\partial x} = -\frac{f}{2}\pi\rho_c u D + \rho S g\sin\theta, \tag{10b}$$

$$\rho_c C_p\left(\frac{\partial(ST)}{\partial t} + u\frac{\partial(ST)}{\partial x}\right) = 2\pi R q_w, \tag{10c}$$

In Boussinesq model we have the approximation $\rho = \rho_{\text{init}}(1 - \alpha(T(x,t) - \frac{T_c+T_f}{2}))$; the temperature does not vary much by hypothesis, while in low-Mach model,

larger temperature gradients may appear. In low-Mach model the velocity varies due to a source term which is not present here. In the Boussinesq model, $p = P_0 + \Pi$, with P_0 is constant in both time and space (we may put in it the hydrostatic variation $\Pi'_{hydrostatic}(x) = -\rho_{\text{init}} g \sin\theta$), whereas, in low-Mach model, it is only constant in space.

3 Reference steady analytical solutions

3.1 The steady solution for one pipe

The system of equations (4), which defines the low-Mach-number averaged model, admits a steady-state solution under a set of simplifying assumptions. First, the nonlinear convective term $\partial_x(\rho u^2)$ is neglected, which is a reasonable approximation for slow flows. Additionally, the flow is assumed to be laminar, with friction modeled as linear in velocity. A constant kinematic viscosity is also assumed, implying $\mu \propto \rho$, and the friction factor is given by $f = \frac{8\nu}{R}$. Under these assumptions, the steady-state equations reduce to:

$$Q'(x) = B(T, P_\infty) q_w(x), \tag{11a}$$

$$\Pi'(x) = \left(-\frac{f}{RS} Q(x) - g \sin\theta \right) \rho(x), \tag{11b}$$

$$Q(x) \frac{T'(x)}{T(x)} = B(T, P_\infty) q_w(x), \tag{11c}$$

where $Q := Su$ denotes the velocity flux, and $B(T, P_\infty)$ is the coefficient defined in (6). We will first derive local solutions for individual pipe segments and subsequently extend the analysis to a complete thermosyphon system.

Considering a generic pipe of length L (x takes values in the interval $[0, L]$) with inlet temperature, flux, and dynamic pressure respectively $T(x = 0)$, $Q(x = 0)$, and $\Pi(x = 0)$, a reference temperature at the wall T_{ref} for non-adiabatic pipes, the solutions of (11) for this pipe are:

$$T(x) = T_{ref} + (T(x = 0) - T_{ref}) e^{-\frac{x}{\lambda}}, \quad Q(x) = \Gamma T(x), \tag{12}$$

$$\Pi(x) = -\frac{\lambda P_\infty g \sin\theta}{\mathrm{r} T_{ref}} (\ln T(x) - \ln T(x = 0)) - \frac{P_\infty}{\mathrm{r} T_{ref}} \left(\frac{f}{RS} T_{ref} \Gamma + g \sin\theta \right) x + \Pi(x = 0). \tag{13}$$

The parameter Γ represents the mass flow rate and the equivalent length λ representis the thermal entry length. They are defined as follows:

$$\Gamma := \frac{Q(x = 0)}{T(x = 0)}, \qquad \lambda := -\frac{\Gamma}{B(T, P_\infty) h}, \text{ or } \lambda = \frac{C_p}{2\pi R h} \frac{P_\infty \Gamma}{\mathrm{r}}. \tag{14}$$

Notice that the constant thermodynamic pressure P_∞ appears in a steady regime. In the case of an adiabatic pipe with inclination $\theta = 0$, the solution reduces to:

$$T(x) = T(x=0), \qquad Q(x) = Q(x=0), \qquad \Pi(x) = -\frac{P_\infty}{\mathrm{r}}\frac{f}{RS}\Gamma x + \Pi_{IN}.$$

3.2 The steady analytical solution for low-Mach model for a thermosyphon

Here, we extend the previous steady analytical solution valid for each pipe to the thermosyphon with four pipes. Starting from the first pipe with $T_0 = T(x=0)$, this pipe is heated at temperature $T_{ref} = T_c$, then at its end the temperature is $T_1 = T(x=L)$. This temperature T_1 is constant in the second pipe (the upper adiabatic one). Then for the third pipe $T_1 = T(x=2L)$ and this pipe is cooled at $T_{ref} = T_f$. At the end of this third pipe, and in the fourth (adiabatic) pipe, the temperature is by periodicity T_0. See figure (1) for clarity. Using (12) we can then express the temperatures T_0 and T_1 as functions of λ :

$$T_1 = \frac{T_c e^{\frac{L}{\lambda}} + T_f}{e^{\frac{L}{\lambda}} + 1}, \quad T_0 = \frac{T_f e^{\frac{L}{\lambda}} + T_c}{e^{\frac{L}{\lambda}} + 1}, \quad \frac{T_0}{T_1} = \frac{T_f e^{\frac{L}{\lambda}} + T_c}{T_c e^{\frac{L}{\lambda}} + T_f}. \tag{15}$$

The conservation of the mass in space imposes the ratio between velocity and temperature to be constant throughout the thermosyphon due to periodicity of the domain. Defining Q_0 in fourth and Q_1 in second:

$$\Gamma = \frac{Q_0}{T_0} = \frac{Q_1}{T_1}.$$

Consequently, Γ and λ are global unknowns with the same value on each pipe.

The conservation of the mass in time imposes that the integral of the density over the domain in the stationary regime is equal to that of the density in the initial state (we define initial conditions by a subscript, for example ρ_{init}). We have by global mass conservation:

$$\int_0^{4L} \rho \mathrm{d}x = \int_0^{4L} \rho_{\text{init}} \mathrm{d}x. \tag{16}$$

The right hand side comes from initial condition and is just $\frac{P_{\text{init}}}{\mathrm{r}T_{\text{init}}} 4L$. The left-hand side can be rewritten and decoupled, by computing all the integrals in each pipe and making some manipulations, we can write equation (16) as :

$$\frac{P_\infty}{P_{\text{init}}}\frac{\lambda}{L}T_{\text{init}}\left(\frac{L}{\lambda}\left(\frac{1}{T_c}+\frac{1}{T_f}+\frac{1}{T_0}+\frac{1}{T_1}\right)+\ln\frac{T_1}{T_0}\left(\frac{1}{T_c}-\frac{1}{T_f}\right)\right) = 4. \tag{17}$$

We need another relation to close the system. For that, we impose that the value of Π at the outlet of the first pipe is equal to the value of Π at the inlet of the second pipe, and so on to obtain a second expression (18). Indeed, using (13) the continuity condition between the first and second pipes is:

$$\Pi_1 = -\frac{g\lambda P_\infty}{\mathrm{r}T_c}\ln\frac{T_1}{T_0} - \frac{P_\infty L}{\mathrm{r}T_c}(\frac{f}{RS}T_c\Gamma + g) + \Pi_0;$$

while between the second and the third $\Pi_2 = \Pi_1 - \frac{P_\infty f L\Gamma}{\mathrm{r}RS}$. The other two continuity conditions are similar. Combining all the continuity conditions, we have:

$$\frac{gRS}{f\Gamma}\left(\frac{\lambda}{L}\ln\frac{T_1}{T_0}\left(\frac{1}{T_c}+\frac{1}{T_f}\right) - \left(\frac{1}{T_f}-\frac{1}{T_c}\right)\right) + 4 = 0. \tag{18}$$

The system (17)-(18) has to be solved to obtain the final solution. But they are highly non-linear and it is not possible to decouple them. Nevertheless we can combine these equations to generate a new one that is a function of only λ. To simplify this last expression we introduce a parameter without dimension G_1

$$G_1 = \frac{PrGa}{128Nu_D}.$$

which is linked to the Galilei number, Prandtl number and Nusselt number :

$$Ga = \frac{gD^3\rho_{\text{init}}^2}{\mu^2},\ Pr = \mu C_p/k,\ Nu_D = \frac{hD}{k}.$$

Furthermore, we define the dimensionless quantity $\varepsilon := \frac{T_c - T_f}{T_c + T_f}$ (smaller than one by definition). Combining (17) and (18) by exploiting (15) gives the final transcendental dimensionless relation linking all the quantities:

$$1 - \frac{G_1 D}{\lambda}\varepsilon + \frac{1-\varepsilon^2}{1-\varepsilon^2\tanh^2\frac{L}{2\lambda}} - \frac{\lambda}{L}\left(\varepsilon - \frac{G_1 D}{\lambda}\right)\ln\left(1 + 2\varepsilon\frac{\tanh\frac{L}{2\lambda}}{1-\varepsilon\tanh\frac{L}{2\lambda}}\right) = 0. \tag{19}$$

The procedure we follow to find the unknown parameters consists in finding λ solving equation (19), then constructing T_0 and T_1 by using (15) and finally computing Γ and P_∞ by using equations (18) and (14).

We can use an iterative approach such as the Newton method to numerically solve equation (19). After computing all the unknowns, the reference solution is ready to validate the numerical results.

3.3 Linearized solution

When the difference of temperatures between heated and cooled wall is small, i.e. when $\varepsilon \ll 1$, a Taylor expansion of the previous relation (19) is:

$$\frac{2}{G_1}\frac{\lambda}{D} + \varepsilon\left(2\frac{\lambda}{L}\tanh\frac{L}{2\lambda} - 1\right) +$$

$$+\varepsilon^2\left(-2\frac{\lambda}{L}\tanh^2\frac{L}{2\lambda} + \frac{1}{G_1}\frac{\lambda}{D}\tanh^2\frac{L}{2\lambda} - \frac{2}{G_1}\frac{\lambda}{D}\tanh\frac{L}{2\lambda} - 1\right) = \mathcal{O}(\varepsilon^3). \quad (20)$$

By dominant balance we guess that

$$\frac{2}{G_1}\frac{\lambda}{D} = \mathcal{O}(\varepsilon),$$

so that:

$$\frac{2}{G_1}\frac{\lambda}{D} + \varepsilon\left(2\frac{\lambda}{L}\tanh\frac{L}{2\lambda} - 1\right) = 0. \quad (21)$$

We will see at the end of this section that this equation represents the Boussinesq continuity equation for a thermosyphon.

Exploring other asymptotic limits of (20) shows that $\frac{L}{2\lambda} \to 0$ is not physically possible, as λ and L are at least comparable. The other possibility is $\frac{L}{2\lambda} \to \infty$. Under this assumption, we have that: $\tanh\frac{L}{2\lambda} \approx 1$. As a consequence, we obtain the following linearization for λ:

$$\lambda \approx RG_1\varepsilon.$$

In order to find by linearization the expression of P_∞, equation (17) is rewritten with ε, it gives:

$$1 + \frac{1-\varepsilon^2}{1-\varepsilon^2\tanh^2\frac{L}{2\lambda}} - \frac{\lambda}{L}\varepsilon\log\left(1 + 2\varepsilon\frac{\tanh\frac{L}{2\lambda}}{1-\varepsilon\tanh\frac{L}{2\lambda}}\right) = 2\frac{P_{\text{init}}}{P_\infty}\frac{T_f}{T_{\text{init}}}(1+\varepsilon).$$

By Taylor expansion, it gives :

$$2\left(1 - \frac{P_{\text{init}}}{P_\infty}\frac{T_f}{T_{\text{init}}}\right) - 2\varepsilon\frac{P_{\text{init}}}{P_\infty}\frac{T_f}{T_{\text{init}}} + \varepsilon^2\left(-1 - 2\frac{\lambda}{L}\tanh\frac{L}{2\lambda} + \tanh^2\frac{L}{2\lambda}\right) + \mathcal{O}(\varepsilon^3) = 0.$$

By dominant balance: $1 - \frac{P_i}{P_\infty}\frac{T_f}{T_i} = \mathcal{O}(\varepsilon)$, this gives an estimation of P_∞ by making a balance between the first two terms, obtaining:

$$P_\infty = P_{\text{init}}\frac{T_f}{T_{\text{init}}}(1+\varepsilon) + \mathcal{O}(\varepsilon^2). \quad (22)$$

this last equation is the linear estimation for P_∞ we were searching for. The total variation for P is given by:

$$\Delta P = P_\infty - P_{\text{init}} = P_{\text{init}} \left(\frac{T_f}{T_{\text{init}}}(1+\varepsilon) - 1 \right) + \mathcal{O}(\varepsilon^2).$$

From this expression, one see that if T_{init} is lesser or greater that $\frac{2}{\frac{1}{T_c}+\frac{1}{T_f}}$, then the pressure drop is negative or positive.

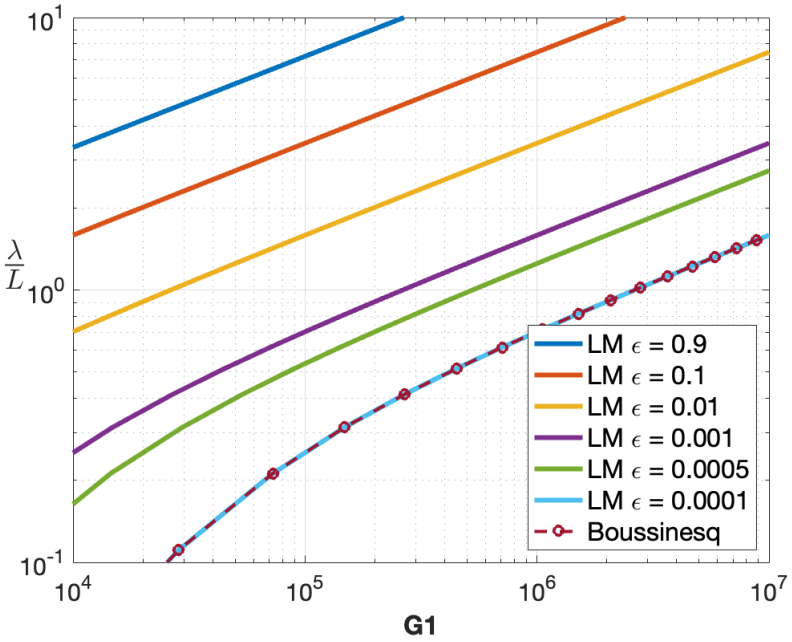

Figure 3: Behavior of the characteristic length λ as a function of the characteristic dimensionless number G_1 by varying the relative temperature rise ε for both the low-Mach and the Boussinesq models.

3.4 Comparison with the classical limit (Boussinesq)

As just suggested when obtaining (21), we may now come back to the Boussinesq model to compare with previous solution of the low-Mach model. To solve the system (10), we also impose continuity conditions for the dynamic pressure along the whole loop: between the first and the second pipes, and between the second and third pipes, they are :

$$\Pi_1 = -\frac{8\mu}{\pi R^4} QL + \alpha \rho_c g \int_0^L (T(x) - T_r) \mathrm{d}x + \Pi_0 \text{ and } \Pi_2 = -\frac{8\mu}{\pi R^4} QL + \Pi_1.$$

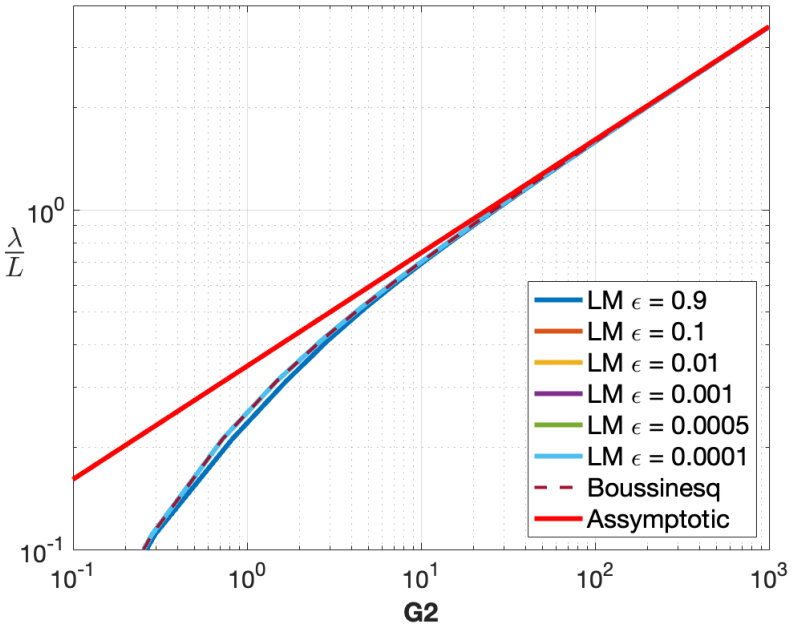

Figure 4: Behavior of the characteristic length λ as a function of the characteristic dimensionless number G_2 by varying the relative temperature rise ε for both the low-Mach and the Boussinesq models. For the low-Mach model, we consider several admissible values of ε, while for the Boussinesq one, we use a small ε. We show the asymptotic limit at infinity.

Similar expressions arise for the other two continuity conditions. Let us now define the Grashof number at the radius scale: $Gr := \alpha \Delta T_c Ga$, with $\Delta T_c = T_c - T_f$, and the Boussinesq counterpart of G_1 as:

$$G_2 = \frac{PrGr}{128Nu_D}\frac{R}{L} = G_1 \alpha \Delta T_c \frac{R}{L} = \varepsilon \frac{G_1 D}{L}.$$

By making the sum of the four equations, we obtain the following final relation, which is the counterpart of equation (19) and which is exactly the equation (21) for $G_1\varepsilon \approx 1$ and ε approach 0:

$$\frac{1}{G_2} = \frac{L}{2\lambda} - \tanh\frac{L}{2\lambda}. \tag{23}$$

So we expect the values we found for λ as a function of G_1 to be the same for both models as $\varepsilon \to 0$. Figure 3 shows how $\frac{\lambda}{L}$ varies as a function of G_1 for different values of ε for a low-Mach model. We see that for small enough values of ε, the results obtained for a low-Mach model coincide with those of a Boussinesq model.

The behavior of λ as a function of G_2 is comparable to that as a function of G_1; the main difference is that, in this case, we see the asymptotic limits. We expect that for $G_1\varepsilon \approx 1$ and consequently $G_2 \approx \frac{D}{L}$ the low-Mach tends to Boussinesq. Moreover, we find a polynomial asymptotic behavior as $\frac{\lambda}{L} \to \infty$. In this case, $\frac{L}{2\lambda} \to 0$ and by exploiting the series expansion of the hyperbolic tangent, equation (23) gives:

$$\frac{\lambda}{L} \approx \frac{1}{\sqrt[3]{24}} G_2^{\frac{1}{3}}.$$

It is possible to see these limit behaviors in figure 4 where we take $L/D = 10$.

4 General algorithm

At this stage we have constructed a low-Mach model and an analytical solution for the simulation of a gas flow throughout a thermosyphon. An algorithm is here proposed for a numerical simulation. Let us remind the final system, equations we want to solve with $0 \leq x \leq 4L$ and $t > 0$ are:

$$s_x := \frac{\partial u}{\partial x} = -\frac{1}{\gamma P(t)} \left(P'(t) + \frac{2\pi R(\gamma - 1)}{S} q_w \right), \tag{24a}$$

$$\partial_t u + u\partial_x u + \frac{\partial_x \Pi}{\rho} = -\frac{f}{2}\pi u \frac{D}{S} - g\sin\theta, \tag{24b}$$

$$P'(t) = -\frac{2\pi R(\gamma - 1)}{S|\Omega|} \int_\Omega q_w, \tag{24c}$$

$$\rho C_p \left(\frac{\partial (ST)}{\partial t} + u \frac{\partial (ST)}{\partial x} \right) = SP'(t) - 2\pi R q_w, \tag{24d}$$

$$q_w := h(T - T_{ref}). \tag{24e}$$

The resulting system consists of four equations for the four unknowns u, T, Π, and P, supplemented by the closure relation for q_w and the equation of state for the density. It is important to note, however, that the model does not explicitly include an evolution equation for Π. Instead, Π must be determined so that the quasi-incompressibility constraint is satisfied. In this framework, Π acts as a Lagrange multiplier ensuring that the velocity field satisfies this constraint, leading to an elliptic equation derived from the momentum equation.

In the following, we construct a coupled numerical algorithm, in which we put together several discretization techniques. Even if every technique is well known by itself, we propose a way to combine them that takes advantage of the best features of each of them. The mesh and the numerical scheme are based on a staggered grid approach, where Π is defined at cell centers, while ρ and T are defined at the interfaces, together with the velocity (see Figure 5). This approach is chosen

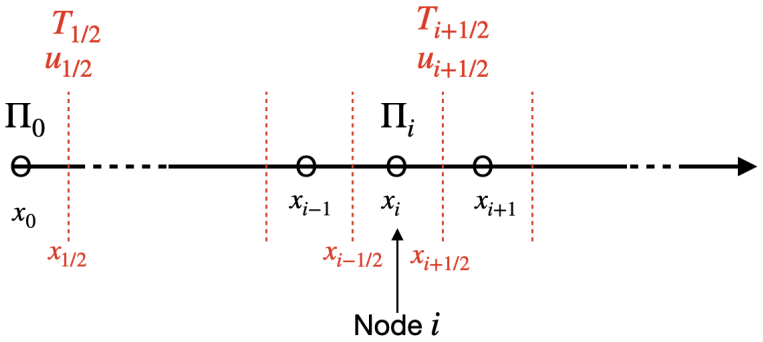

Figure 5: Placement of our variables on the mesh: velocities and temperature at the center of the cells $i \pm \frac{1}{2}$ while dynamic pressure at the nodes i .

to enable a simple and explicit discretization of the convective terms in the mass and momentum equations (see [2, 5, 15, 49]). Alternatively, one could also retain a velocity-pressure/density formalism and apply an interpolation for the density during the correction step.

The algorithm is the following.

Algorithm for T

We apply the method of characteristics [42] described to the equation (24d). We express equation (24d) on every pipe as:

$$\begin{aligned} \frac{\partial T(x,t)}{\partial t} + u(x,t)\frac{\partial T(x,t)}{\partial x} &= f(x,t) \quad \forall x \in [0,L], t \in (0,T], \\ T(x,0) &= T_i(x) \quad \forall x \in [0,L], \\ T(0,t) &= T_0(t) \quad \forall t \in (0,T]. \end{aligned}$$

where $T_i \in \mathcal{L}^\infty([0,L]), T_0 \in \mathcal{L}^\infty((0,T])$ and:

$$f(x,t) = \frac{1}{\rho C_p}P'(t) - \frac{2\pi R}{C_p \rho S}q_w = \frac{(\gamma-1)T(x,t)}{\gamma P(t)}P'(t) - \frac{2h\pi R(\gamma-1)T(x,t)}{S\gamma P(t)}(T(x,t)-T_{ref}).$$

Set the temperature at the foot of the characteristic, $\hat{T}^n := T(\zeta_i^n, t^n)$, and the discrete field $T^n \approx T(\cdot, t^n)$. We choose the following fully discretized scheme:

$$T_{i+1/2}^{n+1} = \frac{\hat{T}_{i+1/2}^n + T_{i+1/2}^n \Delta t \left(\frac{(\gamma-1)}{\gamma P(t^n)} P'(t^n) + \frac{2\pi R(\gamma-1)h}{\gamma S P(t^n)} T_{ref} \right)}{1 + \Delta t \frac{2\pi R(\gamma-1) T_{i+1/2}^n h}{\gamma S P(t^n)}}.$$

Computation of the integral of q_w

Supposing the temperature is regular enough, a good approximation of its integral over the domain derives by the trapezoidal rule:

$$\int_\Omega q_w^{n+1} \mathrm{d}x = \int_\Omega h(T^{n+1} - T_{ref})\mathrm{d}x \approx \sum_{i=0}^{N-1} h(T_{i+1/2}^{n+1} - T_{ref})\Delta x.$$

Computation of P

Thanks to the discretization of the integral of q_w we discretize (24c) via the following implicit Euler scheme:

$$P^{n+1} = P^n - \Delta t \frac{2\pi R(\gamma - 1)}{S|\Omega|} \int_\Omega q_w^{n+1} \mathrm{d}x.$$

Computation of s_x

Equation (24a) can be rewritten as:

$$s_x = \frac{2\pi R(\gamma - 1)}{\gamma S P} \left(\frac{1}{|\Omega|} \int_\Omega q_w \mathrm{d}x - q_w \right).$$

Thanks to the definition of T at the interface $i + \frac{1}{2}$, a discrete expression for s_x can be written as:

$$s_{x\ i+1/2}^{n+1} = \frac{2\pi R(\gamma - 1)}{\gamma S P^{n+1}} \left(\frac{1}{|\Omega|} \int_\Omega q_w^{n+1} \mathrm{d}x - q_{w_{i+1/2}^{n+1}} \right). \tag{25}$$

Computation of Π and u

We apply a projection-correction scheme to solve the coupled problem in veocity-pressure using the formalism of Chorin-Temam. To do so, we introduce an intermediate velocity u^* and use the quasi-incompressibility constraint $\partial_x u = s_x$ at time $n + 1$ computed with (25). We use a time semi-discretization and split the equation (24b) into two parts: :

- Prediction step :

$$\frac{u^* - u^n}{\Delta t} + u^n {s_x}^{n+1} = -f\pi u^* \frac{R}{S}, \tag{26}$$

- Correction step :

$$\frac{u^{n+1}-u^*}{\Delta t} = -\frac{1}{\rho^{n+1}}\frac{\partial \Pi^{n+1}}{\partial x} - g\sin\theta. \tag{27}$$

Equation for Π By applying the divergence operator to the correction step (27), we derive an elliptic equation governing Π. Note the presence of $\sin\theta$, which represents the inclination of the pipe. In the case of a thermosiphon, this inclination can vary from one section to another, leading to a discontinuity. As a result, a Dirac delta appears in the right-hand side of the equation for the pressure.

$$-\partial_x\left(\frac{1}{\rho}\frac{\partial \Pi}{\partial x}\right) = g\sum_{j=1}^{4}\xi_j\delta_{\hat{x}_j} + \frac{1}{\Delta t}(\partial_x u^* - {s_x}^{n+1}). \tag{28}$$

The elliptic equation is discretized and solved using a Finite Volume Method. Using the relation (1d), we introduce $\bar{T}_{i+1/2}$, the value of the temperature, which must be recomputed at cell interfaces for use in the pressure equation scheme. The scheme for the pressure reads at node i centered on the cell $K_i = [x_{i-1/2}, x_{i+1/2}]$:

$$-\frac{\bar{T}_{i-1/2}}{\Delta x_i}\Pi_{i-1} + \frac{\bar{T}_{i-1/2}+\bar{T}_{i+1/2}}{\Delta x_i}\Pi_i - \frac{\bar{T}_{i+1/2}}{\Delta x_i}\Pi_{i+1} = b_i, \tag{29}$$

with b_i is defined as:

$$b_i = g\sum_{j=1}^{4}\bar{\xi}_j\delta_{i(j),i} + \frac{P}{r\Delta t}((u^*_{i+1/2}-u^*_{i-1/2}) - \Delta x_i\ {s_x}_i^{n+1}). \tag{30}$$

where $i(j)$ denotes the index i of the mesh node at which the j-th discontinuity, corresponding to the inclination at $\hat{x}_j$ is located. At a given node i, and following the approach proposed in [9] to handle the piecewise nature of the temperature, we have to estimate the temperature at the interface, typically through harmonic averaging :

$$\bar{T}_{i+1/2} = \frac{2\bar{T}_i\bar{T}_{i+1}}{\bar{T}_i+\bar{T}_{i+1}},$$

with $\bar{T}_i$ which can be estimated at node i by $\bar{T}_i = (T_{i+1/2}+T_{i-1/2})/2$. Similarly, for $i \in \{1,2,3,4\}, \bar{\xi}_j$ has to be estimated with a method based on the same work [9, 17]. For a discontinuity located at a node i such that $i = i(j)$, we have :

$$\bar{\xi}_j = \frac{\bar{T}_i}{\bar{T}_{i+1}+\bar{T}_i}\xi_j.$$

where ξ_j represents the corresponding amplitude coefficients $\partial_x(\sin\theta) = \sum_{j=1}^{4} \xi_j \delta(x - \hat{x}_j)$. Owing to the use of a staggered grid, with the temperature defined at cell interfaces, u^* is naturally evaluated at $i + 1/2$ and directly provided by the prediction step. (26). In the context of the 1D model considered here, the chosen strategy has the advantage of being straightforward to implement and is particularly well-suited for network-based coupling, as planned in future developments.

5 Numerical results

Let us briefly show the methodology used to analyze the numerical results obtained by implementing our algorithms on a standard Linux i7-9850H CPU. We start by showing the convergence results in space. Then we compare the numerically computed T, u, P and Π with the reference solution. We do that at the final time the numerical curves converge to a stationary solution. Finally, we analyze what happens by varying some of the physical parameters of the problem. We summarize in Table 2 the physical parameter we used.

Table 2: Physical parameter values used in the numerical results.

Description	**Symbol**	**Value**	**Unit**
Loop length	L	0.125	m
Pipe diameter	D	0.03	m
Cold temperature	T_c	300.15	K
Fluid temperature	T_f	260.15/280.15	K
Thermal conductivity	k	0.0224	$\mathrm{kg{\cdot}m{\cdot}s^{-3}{\cdot}K^{-1}}$
Dynamic viscosity	μ	1.66×10^{-5}	$\mathrm{kg{\cdot}m^{-1}{\cdot}s^{-1}}$
Specific heat at constant pressure	C_p	1039	$\mathrm{m^2{\cdot}s^{-2}{\cdot}K^{-1}}$
Heat capacity ratio	γ	1.4	–
Courant–Friedrichs–Lewy number	CFL	4	–

Figure 6 shows the order of convergence of our algorithms. It confirms that our algorithms are of the first order in space for temperature and velocity.

Figures 7, 8, and 9 show the typical results obtained for pressure and velocity. Let us notice that the numerical solution is well-superposed to the reference one, the profile of temperature and velocity is the same up to a scale factor, and the global variation of speed is small, as expected. We also notice that the dynamic

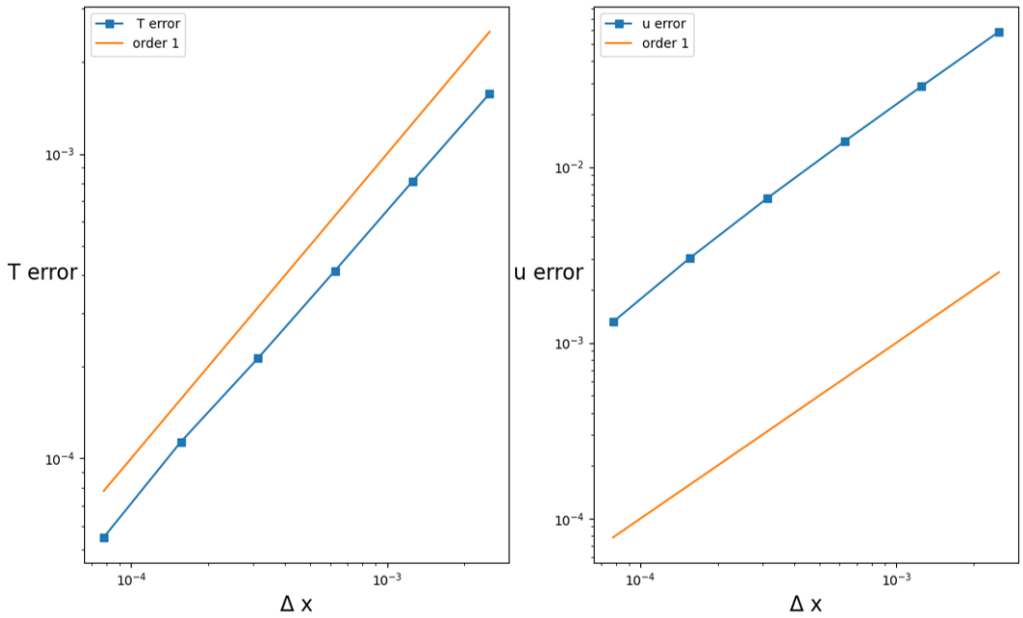

Figure 6: Performance analysis : Error profile for temperature and velocity for a laminar flow at small velocities through a thermosyphon with total length $L = 0.25m$, diameter $D = 0.03m$, and imposed temperatures at the walls $T_c = 300.15K$ and $T_f = 260.15K$.

pressure in the adiabatic pipes is linear with a small slope, almost constant. This slope becomes more significant with smaller values of the radius.

Figure 10 shows the behavior of the thermodynamic pressure P as a function of time. In this case, we change some physical parameters. We take $T_c = 300.15K$ and $T_f = 290.15K$ so that ε is small enough. We take $L = 8m$ to assure that the condition $L > 2\lambda$. We consider two different sets of initial values for thermodynamic pressure and temperature. In a first case $P_i = 202650Pa$, $T_i = 293.07K$ so that $P_\infty > P_i$. In a second case $P_i = 205416Pa$, $T_i = 297.07K$ so that $P_\infty < P_i$. We have chosen the initial values so that the ratio $\frac{P_i}{T_i}$ is the same. This choice allows us to have the same asymptotic stationary estimations. We see that for large enough values of t, they tend asymptotically after an oscillation to the stationary value we computed through the analytical solution.

Figure 11 shows how the temperature varies along x with the conductivity k. The reference temperatures are reached faster as k becomes bigger. Notice that only for sufficiently large values of k the reference temperatures are attained. Moreover, the Péclet number varies between 42.29 and 178.70 for values of k between 0.0124 and 0.0524. Here, we have $L = 1m$.

Table 3 shows the values of the dimensionless number characteristic of the

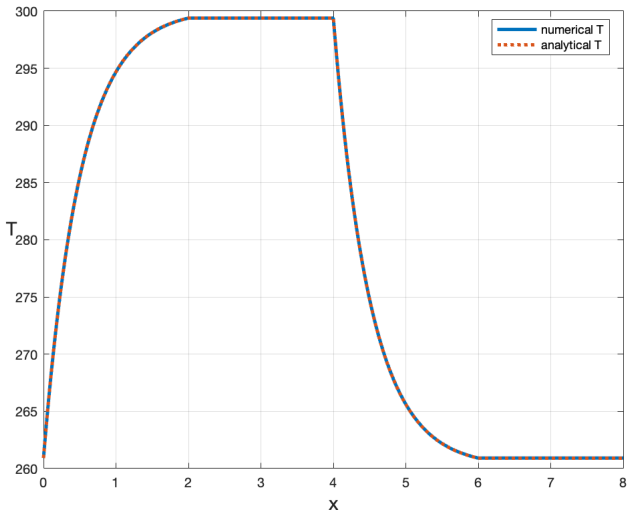

Figure 7: Comparison between the reference solution (in red) and the converged numerical solution (in blue) for the temperature for a laminar flow at small velocities through a thermosyphon with as a number of nodes $N_x = 100000$, final time $T = 10s$, length $L = 2m$, imposed temperatures at the walls $T_c = 300.15K$ and $T_f = 260.15K$, $CFL = 4$.

problem. Notice that the value of Reynolds matches the assumption of laminar flow and that the value of the Mach number is small. Given that the relative temperature difference ε is 0.0345, the values of G_1 and G_2 tell us how far we are from the Boussinesq regime. This is confirmed by the product $G_1\varepsilon$ which is of order 10^2, far from 1 and by the ratio diameter to length D/L, which is 0.03, far from G_2. Notice that, thanks to the low-Mach model, we can take a temperature difference as large as we want, and, thanks to the characteristics method, we can take a CFL condition bigger than 1.

Table 3: The values of the dimensionless numbers characteristic of a laminar flow at small velocities through a thermosyphon with total length $L = 1m$, diameter $D = 0.03m$, and imposed temperatures at the walls $T_c = 300.15K$ and $T_f = 280.15K$.

Re	Ma	Pr	Nu	Pe	Ga	Gr	G_1	G_2
128.48	$1.67\ 10^{-4}$	0.77	3.66	95.08	$1.38\ 10^{6}$	$9.52\ 10^{4}$	$2.27\ 10^{3}$	2.35

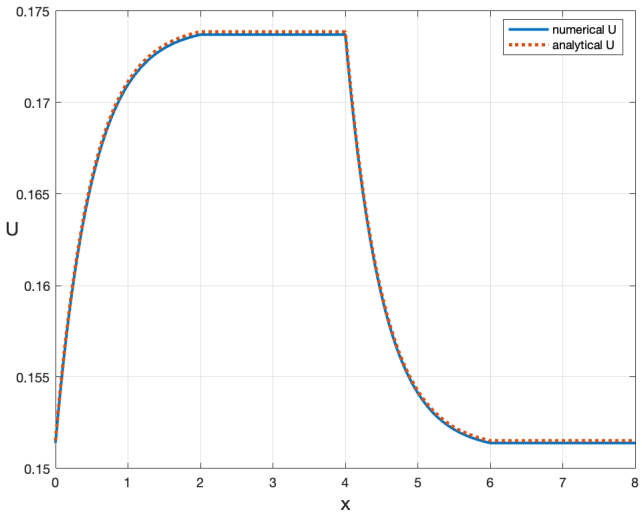

Figure 8: Comparison between the reference solution (in red) and the converged numerical solution (in blue) for the velocity for a laminar flow at small velocities through a thermosyphon with as a number of nodes $N_x = 100000$, final time $T = 10s$, length $L = 2m$, imposed temperatures at the walls $T_c = 300.15K$ and $T_f = 260.15K$, $CFL = 4$.

6 Conclusions and future developments

We focused on the physical modeling and numerical simulation of gas flows at low velocities, with an eye toward engineering applications such as temperature-driven laminar flows in closed pipeline configurations. Our study was based on the one-dimensional, averaged, compressible Navier–Stokes equations under the low-Mach-number approximation, following the formulation proposed by Paolucci. Initially, we assumed a stationary laminar regime and neglected the nonlinear advection term, enabling us to derive a quasi-analytical solution to the fully coupled system. We compared this low-Mach model to its counterpart the classical Boussinesq approximation, demonstrating that the former offers a more accurate representation of the underlying physics. Subsequently, we developed a coupled numerical algorithm for the full set of governing equations, primarily using finite difference schemes. We also designed an algorithm to solve the characteristic equations and employed it to compute the temperature field and constructed a linear system to solve the elliptic equation governing the dynamic pressure.

Although a detailed comparison with experimental data is beyond the scope of this paper, it remains a promising direction for future work. Such a study would involve benchmarking the numerical solutions obtained here with experimental

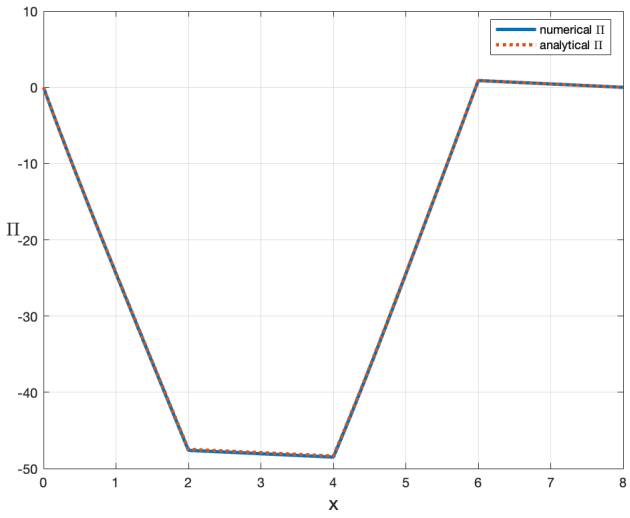

Figure 9: Comparison between the reference solution (in red) and the converged numerical solution (in blue) for the dynamic pressure for a laminar flow at small velocities through a thermosyphon with as a number of nodes $N_x = 100000$, final time $T = 10s$, length $L = 2m$, imposed temperatures at the walls $T_c = 300.15K$ and $T_f = 260.15K$, $CFL = 4$.

results for looped thermosiphon configurations, using different solvers and physical models (eg: 2D Boussinesq with FreeFem++ and 3D models with OpenFOAM. However, the primary focus of this paper is to establish an analytical reference solution, which provides a clear framework for understanding the low Mach number gas flows in these networks.

From the numerical point of view, it would be possible to enrich the algorithms to make them more efficient, for example, by using second-order schemes. It could also be possible to try techniques like finite elements, finite volumes methods, spectral methods instead of finite differences. Possible future developments could be the analysis of a turbulent regime, which presents no difficulties in the 1D framework and extending the algorithm to pipeline networks. The numerical algorithm is adapted to the extension to configurations with more pipes if conditions at the junctions are taken into consideration. Moreover, we must also consider an extension to a non-ideal gas, to non-constant $C_p(T)$ or $\nu(T)$, to the non-constant cross-section and non-cylindrical pipes.

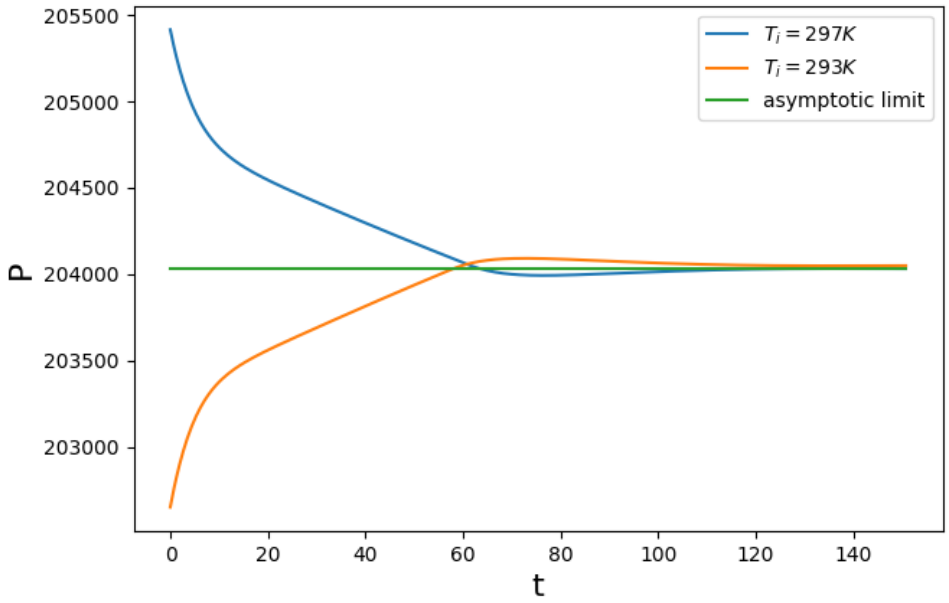

Figure 10: Two examples of thermodynamic pressure profiles for a laminar flow at small velocities through a thermosyphon as a function time with as a number of nodes $N_x = 25597$, final time $T = 150s$, total length $L = 8m$, imposed temperatures at the walls $T_c = 300.15K$ and $T_f = 290.15K$, so that $\varepsilon = 0.017$. For the orange pressure $P_i = 202650Pa$ and $T_i = 293.07K$, while for the blue one $P_i = 205416Pa$ and $T_i = 297.07K$.

References

[1] Gilbert Accary and Isabelle Raspo. A 3d finite volume method for the prediction of a supercritical fluid buoyant flow in a differentially heated cavity. Computers & Fluids, 35(10):1316–1331, 2006.

[2] Nora Aissiouene, Marie-Odile Bristeau, Edwige Godlewski, and Jacques Sainte-Marie. A combined finite volume - finite element scheme for a dispersive shallow water system. Networks and Heterogeneous Media, 11(1):1–27, January 2016.

[3] W. Arfaoui, M. Safi, and P.-Y. Lagrée. Buoyancy-aided convection flow in a heated straight pipe: comparing different asymptotic models. Heat and Mass Transfer, pages 1–13, 2015.

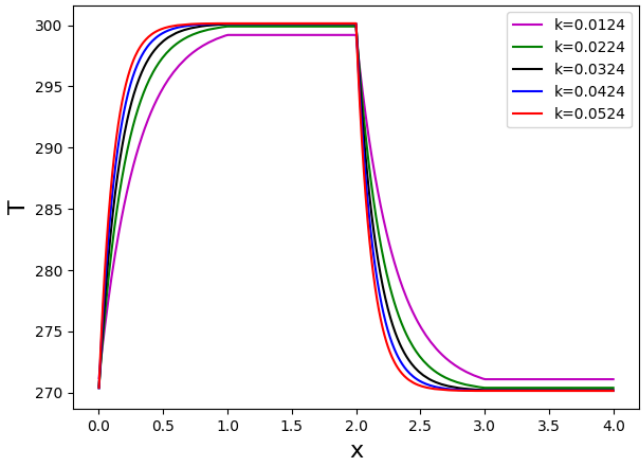

Figure 11: Temperature profile for a laminar flow at small velocities through a thermosyphon by varying the conductivity k with as the number of nodes $N_x = 3997$, final time $T = 10s$, length $L = 1m$, imposed temperatures at the walls $T_c = 300.15K$ and $T_f = 280.15K$. The Péclet number varies between 42.29 and 178.70 for values of k between 0.0124 and 0.0524.

[4] Federico Dalla Barba, Nicoló Scapin, Andreas D. Demou, Marco E. Rosti, Francesco Picano, and Luca Brandt. An interface capturing method for liquid-gas flows at low-mach number. Computers & Fluids, 216:104789, 2021.

[5] John B. Bell and Daniel L. Marcus. A second-order projection method for variable-density flows. Journal of Computational Physics, 101(2):334–348, 1992.

[6] M.A. Bernier and B.R. Baliga. A 1-d/2-d model and experimental results for a closed-loop thermosyphon with vertical heat transfer sections. International Journal of Heat and Mass Transfer, 35(11):2969–2982, 1992.

[7] Ouafa Bouloumou, Eric Serre, Patrick Bontoux, and Jochen Fröhlich. A 3d pseudo-spectral low mach-number solver for buoyancy driven flows with large temperature differences. Computers & Fluids, 66:107–120, 2012.

[8] J. Boussinesq. Théorie analytique de la chaleur. Gauthier-Villars, 1903.

[9] F. Boyer. Méthodes de volumes finis pour les écoulements en milieux poreux. Laboratoire d'Analyse, Topologie et Probabilités CNRS / Université Paul Cézanne, 2010.

[10] J. Brouwer, I. Gasser, and M. Herty. Gas pipeline models revisited: model hierarchies, nonisothermal models, and simulations of networks. Multiscale Model. Simul., 9:601–623, 2011.

[11] A.A. Chehade, H. Louahlia-Gualous, S. Le Masson, I. Victor, and N. Abouzahab-Damaj. Experimental investigation of thermosyphon loop thermal performance. Energy Conversion and Management, 84:671–680, 2014.

[12] Hardy Cross. Analysis of flow in networks of conduits or conductors. University of Illinois. Engineering Experiment Station. Bulletin; no. 286, 1936.

[13] Gilles Desrayaud, Alberto Fichera, and Guy Lauriat. Two-dimensional numerical analysis of a rectangular closed-loop thermosiphon. Applied Thermal Engineering, 50(1):187–196, 2013.

[14] J. F. Douglas. Fluid Mechanics. Prentice Hall, 2006. chap. 1 and 10.

[15] Michael Dumbser and Vincenzo Casulli. A conservative, weakly nonlinear semi-implicit finite volume scheme for the compressible navier-stokes equations with general equation of state. Applied Mathematics and Computation, 272:479–497, 1 2016.

[16] K. Ehrhardt and M. C. Steinbach. Kkt systems in operative planning for gas distribution networks. Proc. Appl. Math. Mech., 4:606–607, 2004.

[17] Robert Eymard, Thierry Gallouët, and Raphaèle Herbin. Finite volume methods. Handbook of numerical analysis, 7:713–1018, 2000.

[18] M. Ferreira Santos. Analysis of transient flow in natural gas transmission network. 2010.

[19] Arthur Ghigo, Jose-Maria Fullana, and P.-Y. Lagrée. A 2d nonlinear multiring model for blood flow in large elastic arteries. Journalof Computational Physics, 350:136–165, 2017.

[20] J. C. C. Henriques. Modelação de regimes transitórios lentos em redes de gás usando o método dos elementos finitos. Technical report, IDMEC, 2010.

[21] A. Herrán González, J. De La Cruz, B. De Andrés Toro, and J. Risco Martín. Modeling and simulation of a gas distribution pipeline network. Applied Mathematical Modelling, 33:1584–1600, 2009.

[22] M. Herty, J. Mohring, and V. Sachers. A new model for gas flow in pipe networks. Math. Methods Appl. Sci., 33:845–855, 2010.

[23] O. Hireche, C. Weisman, D. Baltean Carlès, P. Le Quéré, and L. Bauwens. Low mach number analysis of idealized thermoacoustic engines with numerical solution. The Journal of the Acoustical Society of America, 128, 2010.

[24] C. S. Huang, Chia-Wang Yu, R. H. Chen, Chun-Ta Tzeng, and Chi-Ming Lai. Experimental observation of natural convection heat transfer performance of a rectangular thermosyphon. Energies, 12(9), 2019.

[25] Juan Gutiérrez Jorquera and Florian Kummer. A fully coupled high-order discontinuous galerkin method for diffusion flames in a low-mach number framework. International Journal for Numerical Methods in Fluids, 2021.

[26] S. L. Ke and H. C. Ti. Transient analysis of isothermal gas flow in pipeline network. Chem. Eng. J., 76:169–177, 2000.

[27] Sara Kloczko and Amir Faghri. Experimental investigation on loop thermosyphon thermal performance with flow visualization. International Journal of Heat and Mass Transfer, 150:119312, 2020.

[28] P. Le Quéré, C. Weisman, H. Paillère, J. Vierendeels, E. Dick, R. Becker, M. andBraack, and J. Locke. Modelling of natural convection flows with large temperature differences: a benchmark problem for low mach number solvers. part i. reference solutions. ESAIM: Mathematical Modelling and Numerical Analysis, pages 609–616, 2005.

[29] A. Leontiev. Théorie des échanges de chaleur et de masse. Éditions Mir, 1985.

[30] M. Lucchesi, H. H. Alzahrani, C. Safta, and O. M. Knio. A hybrid, non-split, stiff/rkc, solver for advection–diffusion–reaction equations and its application to low-mach number combustion. Combustion Theory and Modelling, 23(5):935–955, 2019.

[31] L. Ma, C. Weisman, D. Baltean Carlès, P. Le Quéré, and L. Bauwens. Low mach number simulation of a loaded standing-wave thermoacoustic engine. Acoustics, 2012, Nantes, France.

[32] Andrew Majda and James Sethian. The derivation and numerical solution of the equations for zero mach number combustion. Combustion Science and Technology, 42(3-4):185–205, 1985.

[33] B. S. Massey. Mechanics of Fluids. Van Nostrand Reinhold Inc.,U.S., 4^{th} edition, 1978 (1^{st} edition). chap. 1 and 6.

[34] D. Matko, G. Geiger, and W. Gregoritza. Pipeline simulation techniques. Math. Comput. Simul., 52:211–230, 2000.

[35] A. Nonaka, J. B. Bell, M. S. Day, C. Gilet, A. S. Almgren, and M. L. Minion. A deferred correction coupling strategy for low mach number flow with complex chemistry. Combustion Theory and Modelling, 16(6):1053–1088, 2012.

[36] A. J. Osiadacz. Simulation and Analysis of Gas Pipeline Networks. E.& F.N. Spon, London, 1987.

[37] A. J. Osiadacz and M. Chaczykowski. Comparison of isothermal and non-isothermal pipeline gas flow model. Chem. Eng. J., 81:41–51, 2001.

[38] H. Paillere, C. Viozat, A. Kumbaro, and et al. Comparison of low mach number models for natural convection problems. Heat and Mass Transfer, 36:567–573, 2000.

[39] S. Paolucci. On the filtering of sound from the navier-stokes equations. 1982.

[40] S. Paolucci. The differential heated cavity. Sadhana, 19(5):619–647, 1994.

[41] Will E. Pazner, Andrew Nonaka, John B. Bell, Marcus S. Day, and Michael L. Minion. A high-order spectral deferred correction strategy for low mach number flow with complex chemistry. Combustion Theory and Modelling, 20(3):521–547, 2016.

[42] Yohan Penel. Etude théorique et numérique de la déformation d'une interface séparant deux fluides non-miscibles à bas nombre de Mach. Ph. d. thesis, Université Paris-Nord - Paris XIII, 2010.

[43] L. Prandtl. Guide à travers la mécanique des fluides. Dunod, 1952.

[44] H. Prashanth Reddy, Shankar Narasimhan, and S. Murty Bhallamudi. Simulation and state estimation of transient flow in gas pipeline networks using a transfer function model. Ind. Eng. Chem. Res., 45:3853–3863, 2006.

[45] R. Reyes, R. Codina, J. Baiges, and et al. Reduced order models for thermally coupled low mach flows. Adv. Model. and Simul. in Eng. Sci., 5:28, 2018.

[46] K. Sai Sandeep and G. Narendar. Design and thermodynamic analysis of single-loop thermosyphon. In Proceedings of the Second International Conference on Emerging Trends in Engineering (ICETE 2023), pages 1197–1207. Atlantis Press, 2023.

[47] G. Scarella, G. Accary, S. Meradji, D. Morvan, and O. Bessonov. Three-dimensional numerical simulation of the interaction between natural convection and radiation in a differentially heated cavity in the low mach number approximation. ICHMT International Symposium on Advances in Computational Heat Transfer, 2008, Marrakech, Morocco.

[48] H. Schlichting and K. Gersten. Boundary-Layer Theory. Springer, 8th edition, 2000.

[49] Maurizio Tavelli and Michael Dumbser. A pressure-based semi-implicit space-time discontinuous galerkin method on staggered unstructured meshes for the solution of the compressible navier-stokes equations at all mach numbers. 12 2016.

[50] F. De Vita, P.-Y. Lagrée, S. Chibbaro, and S. Popinet. Beyond shallow water: appraisal of a numerical approach to hydraulic jumps based upon the boundary layer theory. European Journal of Mechanics/ B Fluids, 79:233–246, 2020.

[51] Catherine Weisman, Diana G. Baltean Carlès, Patrick Le Quéré, and Luc Bauwens. Modèle Faible Mach et simulations numériques 2D de l'amplification d'onde thermoacoustique. In Société Française d'Acoustique SFA, editor, 10ème Congrès Français d'Acoustique, pages –, Lyon, France, April 2010.

[52] M. Yedrouj and A. J. Osiadacz. A comparison of a finite element method and a finite difference method for transient simulation of a gas pipeline. Appl. Math. Modelling, 13, 1989.

[53] Çengel Yunus. Heat and Mass Transfer, page 480. McGraw-Hill, 2^{nd} edition, 2006.